Density-dependent spin-orbit coupling in degenerate quantum gases

Peng Xu ,[1] Tian-Shu Deng,[1] Wei Zheng,[2,3,*] and Hui Zhai[1,†]

[1]*Institute for Advanced Study, Tsinghua University, Beijing 100084, China*
[2]*Hefei National Laboratory for Physical Sciences at the Microscale and Department of Modern Physics,*
University of Science and Technology of China, Hefei 230026, China
[3]*CAS Center for Excellence in Quantum Information and Quantum Physics,*
University of Science and Technology of China, Hefei 230026, China

In this letter we propose a method to realize a kind of spin-orbit coupling in ultracold Bose and Fermi gases that depends on the density of atoms. Our method combines two-photon Raman transition and periodical modulation of spin-dependent interaction, which gives rise to both the direct Raman process and the interaction-assisted Raman process. The interaction-assisted Raman process depends on the density of atoms. These two processes have opposite effects in terms of spin-momentum locking and compete with each other. As the interaction modulation increases, the system undergoes a crossover from the direct Raman process dominated regime to the interaction-assisted Raman process dominated regime. During this crossover, for bosons, both the condensate momentum and the chirality of condensate wave function change sign, and for fermions, the Fermi surface distortion is inverted. We highlight that there exists an emergent spatial reflectional symmetry in the crossover regime, which can manifest itself universally in both Bose and Fermi gases. Our method may pave a way to novel phenomena in the density-dependent spin-orbit coupling gauge field with intrinsic dynamics.

Introduction. Spin-orbit (SO) coupling is an unambiguous phemonenon of the electron gases in quantum materials, which is essentially a relativistic effect of charged particles. For a given material, both the form and the strength of the SO coupling are fixed [1,2]. Although the atoms are neutral, SO coupling can now be simulated for ultracold atoms by ultilizing the atom-light interactions [3–5]. In the simplest and most widely used setting, a pair of Raman lasers are applied to an ultracold atomic cloud [6–8]. This pair of lasers can flip the spin from down to up, accompanied by a momentum transfer to the right, and simultaneously, can flip the spin from up to down, accompanied by a momentum transfer to the left. In this way, the spin and momentum are coupled, thus it leads to the SO coupling effect. Studying SO coupling in ultracold atomic gases can significantly enrich our understanding of its effects on many-body physics. For instance, the impacts of SO coupling on a Bose gas [9–28] and its interplay with the Bose-Einstein condensation–Bardeen-Cooper-Schrieffer (BEC-BCS) crossover [29–39] are both novel effects revealed by ultracold atomic systems, which have no counterpart in electronic system studied before.

Another unique aspect of SO coupling in ultracold atom systems is that the coupling itself can be made dynamical, where the atoms can give feedback to the form or strength of the SO coupling. There are two approaches to realize such dynamical SO coupling. One approach is to replace the classical Raman lasers with the quantum photon field. For

instance, by strongly coupling the ultracold atoms with the optical cavity field [40–42]. Another approach is to make the SO coupling depending on the atom field itself, for instance, depending on the density of atoms. Here we will focus on the second approach. Actually, for the Abelian case, the density-dependent $U(1)$ gauge field has been proposed [43–45] and realized in ultracold atom systems [46–48]. In this letter, we will show that the density dependence can also be realized in SO coupling as a density-dependent spin-orbit coupling gauge field in both degenerate Bose and Fermi gases.

Setting. First, we consider the configuration where a cloud of ultracold atoms is shined by two counterpropagating Raman beams, as shown in Fig. 1(a) and described in the caption of Fig. 1. The single-particle Hamiltonian of the atoms is given by

$$\hat{H}_0 = -\frac{\hbar^2 \nabla^2}{2m} + \frac{h}{2}\sigma_z + \hbar\Omega\cos(2k_{\mathrm{r}}x - \omega t)\sigma_x. \quad (1)$$

Here h is the Zeeman splitting between spin-up and spin-down, k_{r} the wave number of the lasers, Ω the strength of the Raman process, and ω is the frequency difference between two Raman lasers.

We consider periodically modulating the interaction between two spin components as $g\cos(2\omega t)\hat{n}_\uparrow(\mathbf{r})\hat{n}_\downarrow(\mathbf{r})$. Such a technique of modulating interaction is nowadays quite matured in ultracold atom experiments, specifically, the Chicago group's experiment has shown the entire process of modulating scattering length in a Bose gas can be coherent and reversible, therefore heating in this system can be negligible [46,49,50]. For the situation we consider here, to a very good approximation, $\langle\hat{n}_\uparrow(\mathbf{r}) + \hat{n}_\downarrow(\mathbf{r})\rangle$ is a constant. Therefore, it is

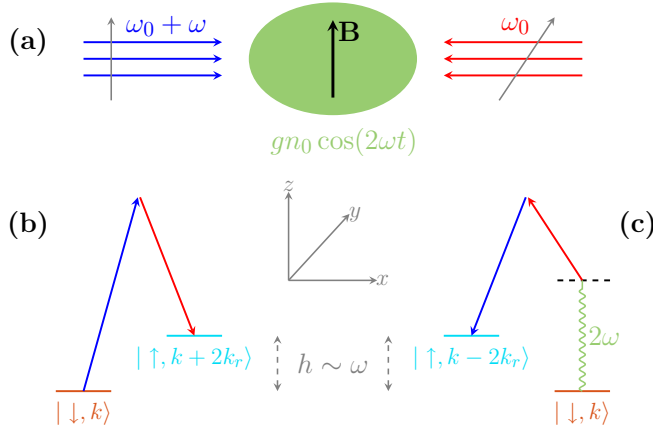*zw8796@ustc.edu.cn
†huizhai.physics@gmail.com

FIG. 1. (a) Schematic of experimental configuration. A pair of Raman lasers propagating along $\hat{x}$ are applied to a cloud of ultracold atoms. One laser is linearly polarized along $\hat{y}$ with frequency ω_0 and the other laser is linearly polarized along $\hat{z}$ with frequency $\omega_0 + \omega$. A Zeeman field is applied along $\hat{z}$ and spin-dependent interaction is modulated with frequency 2ω. (b) Direct Raman transition regime. A two-photon process induces a spin flip σ^+ with momentum transfer $2k_r$. (c) Interaction-assisted Raman transition regime. A two-photon process induces a spin flip σ^+ with momentum transfer $-2k_r$, and the energy offset is compensated by interaction modulation.

convenient to rewrite the interaction Hamiltonian as

$$-\frac{g}{4}\cos(2\omega t)[\hat{n}_\uparrow(\mathbf{r}) - \hat{n}_\downarrow(\mathbf{r})]^2. \tag{2}$$

Here we leave the total density-density interaction for future consideration as it does not enter the Raman processes considered here. We employ the Hartree-Fock mean-field treatment by the approximation $[\hat{n}_\uparrow(\mathbf{r}) - \hat{n}_\downarrow(\mathbf{r})]^2 \approx 2n_0 M_z(\mathbf{r})[\hat{n}_\uparrow(\mathbf{r}) - \hat{n}_\downarrow(\mathbf{r})]$, where $M_z(\mathbf{r}) = \langle \hat{n}_\uparrow(\mathbf{r}) - \hat{n}_\downarrow(\mathbf{r}) \rangle / n_0$ is the normalized magnetization and $n_0 = N/V$ is the average total density. Thus the mean-field single-particle Hamiltonian can be written as

$$\hat{H}_{\mathrm{MF}} = \hat{H}_0 - \frac{g}{2}n_0 M_z(\mathbf{r})\sigma_z \cos(2\omega t), \tag{3}$$

where $\hat{H}_0$ is given by Eq. (1). Note that the magnetization $M_z(\mathbf{r})$ needs to be determined self-consistently.

Floquet methods. We employ the Floquet approach to solve the mean-field Hamiltonian in Eq. (3). One way is to calculate the time evolution operator $\hat{U}(T) = \mathcal{T}\exp\{-i\int_0^T dt\hat{H}_{\mathrm{MF}}(t)/\hbar\}$ for a given $M_z(\mathbf{r})$ numerically. Then we diagonalize the time evolution operator as $\hat{U}(T)|\varphi_n\rangle = e^{-i\varepsilon_n T\hbar}|\varphi_n\rangle$. Here ε_n is the quasi-energy, which is restricted in the regime $-\pi\hbar/T\,\varepsilon_n\,\pi\hbar/T$ and $|\varphi_n\rangle$ is the corresponding Floquet eigenstate. Thus for bosons, we consider that all atoms condense on the state with the lowest quasi-energy, and for fermions, we consider that all atoms fill a Fermi sea. So the magnetization $M_z(\mathbf{r})$ can be obtained according to either the condensation wave function for bosons or the Fermi sea wave function for fermions, respectively. Finally, we substitute this $M_z(\mathbf{r})$ to $\hat{U}(T)$ and solve the Floquet eigenstate iteratively until a self-consistency is reached.

To see the physics more clearly, another way is to obtain the Floquet effective Hamiltonian. First we apply a unitary

rotation $\hat{U}$ to the mean-field Hamiltonian in Eq. (3),

$$\hat{U} = e^{\frac{i}{\hbar}\int_0^t dt'[\frac{\hbar\omega}{2}\sigma_z - \frac{gn_0 M_z}{2}\sigma_z \cos(2\omega t')]}. \tag{4}$$

The Hamiltonian after rotation is given by

$$\begin{aligned}
\hat{H}(t) &= \hat{U}\hat{H}_{\mathrm{MF}}\hat{U}^\dagger - i\hbar\hat{U}\partial_t\hat{U}^\dagger \\
&= -\frac{\hbar^2\nabla^2}{2m} + \delta\sigma_z + \hbar\Omega\cos(2k_r x - \omega t) \\
&\quad \times \begin{pmatrix} 0 & e^{i[\omega t - \frac{\lambda M_z}{2}\sin(2\omega t)]} \\ \mathrm{H.c.} & 0 \end{pmatrix},
\end{aligned} \tag{5}$$

where $\delta = (h - \hbar\omega)/2$ and $\lambda = gn_0/(\hbar\omega)$, which is proportional to the atom density and the modulation amplitude. Here, for simplicity, we assumed that M_z is a spatial-independent constant, which has been well justified by the numerical calculation.

Note that

$$\begin{aligned}
&\cos(2k_r x - \omega t)e^{i[\omega t - \frac{\lambda M_z}{2}\sin(2\omega t)]} \\
&= \frac{e^{i2k_r x} + e^{-i2k_r x + i2\omega t}}{2} \sum_{n=-\infty}^{n=\infty} \mathcal{J}_n\left(-\frac{\lambda M_z}{2}\right)e^{i2n\omega t}, \tag{6}
\end{aligned}$$

where $\mathcal{J}_n$ is the Bessel function of order n. When $\hbar\omega$ is much larger than the typical kinetic energy and the Raman coupling strength of the system, we can use the high-frequency expansion to obtain the Floquet effective Hamiltonian [51,52], $\hat{H}_{\mathrm{eff}} \approx \hat{H}^{(0)} + \sum_{n=1}^\infty \frac{[\hat{H}^{(n)}, \hat{H}^{(-n)}]}{\hbar\omega} + \cdots$, where $\hat{H}^{(n)} = \frac{1}{T}\int_0^T \hat{H}(t)e^{-in\omega t}dt$. In the high-frequency limit, we can keep the expansion to the leading order $\hat{H}_{\mathrm{eff}} \approx \hat{H}^{(0)}$, obtaining

$$\begin{aligned}
\hat{H}_{\mathrm{eff}} &= -\frac{\hbar^2\nabla^2}{2m} + \delta\sigma_z + \frac{\hbar\Omega}{2} \\
&\quad \times \begin{pmatrix} 0 & \mathcal{J}_0\left(\frac{\lambda M_z}{2}\right)e^{i2k_r x} + \mathcal{J}_1\left(\frac{\lambda M_z}{2}\right)e^{-i2k_r x} \\ \mathrm{H.c.} & 0 \end{pmatrix}. \tag{7}
\end{aligned}$$

Discussions of the effective Hamiltonian. The effective Hamiltonian Eq. (7) is a central result of this work. It represents a faithful representation of the density-dependent SO coupling proposed in this work. To illustrate the physics clearly, we first look at two limits.

Note that for low atomic density or small modulation amplitude $\lambda \to 0$, we have $\mathcal{J}_0 \to 1$ and $\mathcal{J}_1 \to 0$. Thus, in this limit, the $\mathcal{J}_0$ term dominates over the $\mathcal{J}_1$ term. If we ignore the $\mathcal{J}_1$ term, this effective Hamiltonian can be transformed into

$$\hat{H}_{\mathrm{eff}} = \frac{\hbar^2}{2m}(-i\nabla + k_r\mathbf{e}_x\sigma_z)^2 + \delta\sigma_z + \frac{\hbar\Omega_0}{2}\sigma_x \tag{8}$$

by a unitary transformation $\hat{U}_0 = e^{-i\sigma_z k_r x}$, where $\Omega_0 = \Omega\mathcal{J}_0(\lambda M_z/2)$. Except for renormalizing Ω to Ω_0, this is the same effective Hamiltonian for the direct Raman process at the single-particle level. This direct Raman coupling term is shown in Fig. 1(b), where the momentum of an atom increases by $2\hbar k_r$ when its spin is flipped from down to up, and decreases by $2\hbar k_r$ when its spin is flipped in an opposite way.

As λ increases, $\mathcal{J}_1$ increases and $\mathcal{J}_0$ is suppressed. For large atomic density or strong modulation, the $\mathcal{J}_1$ term dominates over the $\mathcal{J}_0$ term. If we ignore the $\mathcal{J}_0$ term, the effective

Hamiltonian can be transformed into

$$\hat{H}_{\text{eff}} = \frac{\hbar^2}{2m}(-i\nabla - k_{\text{r}}\mathbf{e}_x\sigma_z)^2 + \delta\sigma_z + \frac{\hbar\Omega_1}{2}\sigma_x \quad (9)$$

by a unitary transformation $\hat{\mathcal{U}}_1 = e^{i\sigma_z k_{\text{r}}x}$, where Ω_1 is given by $\Omega\mathcal{J}_1(\lambda M_z/2)$. Note that $k_{\text{r}}\sigma_z$ in Eq. (8) is now changed to $-k_{\text{r}}\sigma_z$ in Eq. (9). This Hamiltonian actually describes the opposite process compared with the direct Raman transition. As shown in Fig. 1(c), the momentum of an atom decreases by $2\hbar k_{\text{r}}$ when its spin is flipped from down to up; while it will increases by $2\hbar k_{\text{r}}$ when its spin is flipped from up to down. However, at the single-particle level, when $h \sim \hbar\omega$, the energy between the initial and the final states of this process differs by $\sim 2\hbar\omega$. This $2\hbar\omega$ energy offset can be compensated by absorbing one energy quanta from the periodically modulating with a frequency 2ω [53]. Thus, the combination of interaction modulation and Raman beam gives rise to the interaction-assisted Raman process depending on the atomic density.

Therefore, when the atomic density is low, the direct Raman process dominates; while in the large atomic density limit, the interaction-assisted Raman process dominates. Both the strength and the sign of the SO coupling are density dependent. The effective Hamiltonian Eq. (7) includes both processes on equal footing and illustrates clearly the competition between them.

Results for bosons. We consider the ground state of a three-dimensional Bose condensate with $\delta = 0$. In this case, the numerical calculation shows that there are two degenerate ground states where the majority of atoms, either spin-up or spin-down, condense at the momentum of energy minima $\mathbf{k}_{\min} = (k_{\min}, 0, 0)$ around zero. In one of the ground states, in the direct Raman coupling regime, the majority of spin-down atoms are coupled to the minority of spin-up atoms with positive momentum, and therefore, $k_{\min}$ is pushed to a slightly negative value in the direction of Raman lasers. If we define a chirality $\langle \hat{k}\sigma_z \rangle$ with $\hat{k} = k_{\min}/|\mathbf{k}_{\min}|$, the chirality is positive. In the interaction-assisted Raman coupling regime, in contrast, the majority of spin-down atoms are coupled to the minority of spin-up atoms with negative momentum, and therefore, $k_{\min}$ is pushed to a slightly positive value in the direction of Raman lasers. Then the chirality is negative. In the crossover regime, both direct and interaction-assisted Raman processes are equally important, and the minority of spin-up atoms appear at both positive and negative momenta. This is schematically shown in the first row of Fig. 2.

The results obtained from quantitative calculations are shown in Fig. 3, which are obtained by self-consistently solving the Floquet Hamiltonian. We show how the condensation momentum and chirality change when the interaction modulation increases. One can especially see that the chirality jumps from positive to negative at the point where $k_{\min}$ crosses zero. In another degenerate state, the majority of spin-up atoms are coupled to the minority of spin-down atoms with negative momentum in the direct Raman coupling regime, and are coupled to the minority of spin-down atoms with positive momentum in the interaction-assisted Raman coupling regime, as shown in the second row of Fig. 2. Consequently, $k_{\min}$ changes from positive to negative as the interaction modulation increases.
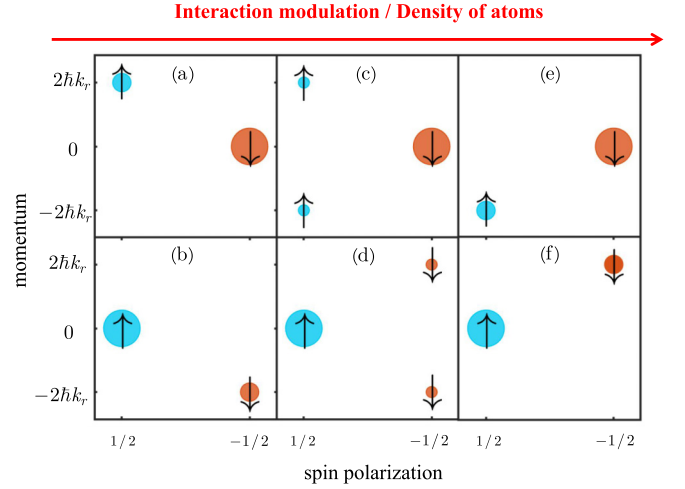

FIG. 2. Schematic of the experimental prediction for spin-resolved momentum distribution. Here blue circles with upper arrows denote the cloud of spin-up atoms, and yellow circles with down arrows denote the cloud of spin-down atoms. The size of the circles is proportional to the atom number. They are separated along the horizontal spatial direction because of the Stern-Gerlach effect. The vertical axes denote different momenta measured by the time of flight. (a), (b) The direct Raman coupling regime, where the interaction modulation amplitude or atomic density are small. (e), (f), The interaction-assisted Raman coupling with large modulation amplitude or atomic density. (c), (d) The crossover regime where both processes are important. For bosons, the prediction is for the detuning $\delta \sim 0$ and two different rows are for two degenerate ground states. For fermions, the upper row is for $\delta \gtrsim E_{\text{F}} > 0$ and the lower row is for $\delta < 0$ and $|\delta| \gtrsim E_{\text{F}}$, where E_{F} is the Fermi energy.
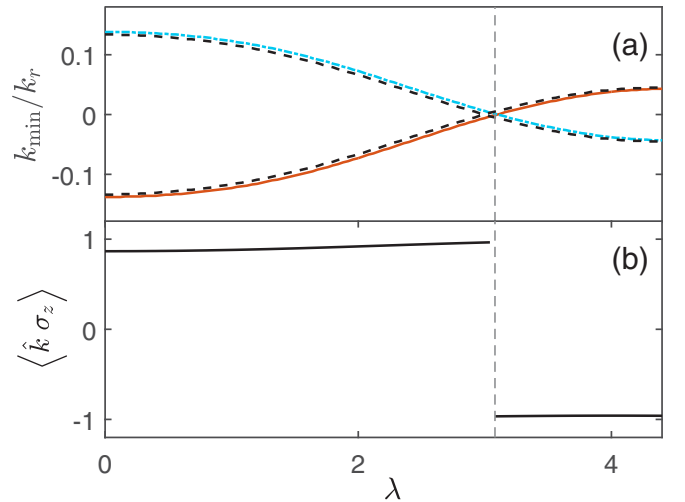

FIG. 3. Bose-Einstein condensate with density-dependent SO coupling. (a) The condensation momentum $k_{\min}$ (in units of k_{r}) as a function of interaction modulation amplitude $\lambda = gn_0/(\hbar\omega)$. Two lines are for two degenerate ground states with $\langle \sigma_z \rangle > 0$ (the dot-dashed line) and $\langle \sigma_z \rangle < 0$ (solid line), respectively. The dot-dashed line and solid line are obtained by numerical calculation, while the dashed lines are obtained by the effective Hamiltonian. (b) The chirality $\langle \hat{k}\sigma_z \rangle$ of the ground state. The two ground states share the same value of chirality. Here we take $\delta = 0$, $\Omega = 2E_r$ and $\omega = 20E_r$, with $E_r = \hbar^2 k_r^2/(2m)$. The vertical gray dashed line denotes the value of λ where $k_{\min} = 0$ and the chirality jumps.
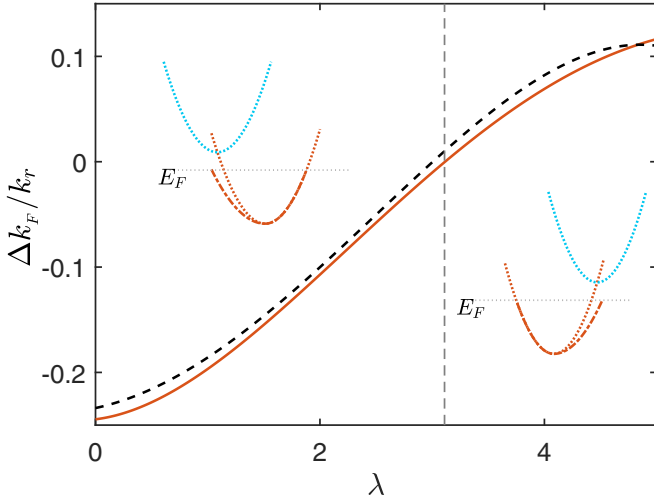
FIG. 4. One-dimensional degenerate Fermi gas with density-dependent SO coupling. $\Delta k_{\rm F} = k_{\rm F}^+ + k_{\rm F}^-$, where $k_{\rm F}^\pm$ are the Fermi points at positive and negative momenta. $\Delta k_{\rm F}$ (in units of $k_{\rm r}$) is plotted as a function of interaction modulation amplitude $\lambda = g n_0/(\hbar\omega)$. The solid line and dashed line are obtained by calculation and the effective Hamiltonian, respectively. The inset schematically shows the distortion of fermion dispersion in the direct Raman coupling regime (left) and the density-assisted Raman coupling regime (right). The dotted lines are dispersion without spin-orbit coupling, while the dot-dashed lines are distorted dispersion. Here we set $\delta = 4.5 E_r$, $\Omega = 2 E_r$, $\omega = 20 E_r$, and $n_0/k_r = 4$. The vertical gray dashed line denotes the value of λ where $\Delta k_{\rm F} = 0$.

The behaviors of the chirality are the same for these two states, as shown in Fig. 3(b).

Results for fermions. For the degenerate Fermi gas, we consider a simpler situation, where fermions are confined in a one-dimensional tube along the direction of the Raman lasers. When $\delta \gtrsim E_{\rm F} > 0$, the majority of fermions are spin-down atoms in the presence of SO coupling. The situation is similar to the first row of Fig. 2, with the only difference that atoms populate a Fermi sea instead of occupying the lowest-energy state. In one dimension, the Fermi surfaces are simply two points whose momenta are denoted by $k_{\rm F}^\pm$ at positive and negative, respectively. Because the Raman process distorts the single-particle dispersion and breaks the spatial reflection symmetry, in general $k_{\rm F}^+ \neq -k_{\rm F}^-$. In Fig. 4 we show $\Delta k_{\rm F} = k_{\rm F}^+ + k_{\rm F}^-$ as a function of the interaction modulation strength. It shows that the direct Raman coupling and the interaction-assisted Raman coupling distort the fermion

dispersion in an opposite way, and therefore, $\Delta k_{\rm F}$ changes from negative to positive when interaction modulation increases. If $\delta < 0$ and $|\delta| > E_{\rm F}$, the majority of fermions are spin-up atoms. The situation behaves as the second row of Fig. 2, and $\Delta k_{\rm F}$ changes from positive to negative when interaction modulation increases.

Emergent Z_2 symmetry. The presence of SO coupling generally breaks the spatial reflection symmetry. However, this symmetry is restored when $\mathcal{J}_0(\lambda M_z/2) = \mathcal{J}_1(\lambda M_z/2)$. As one can see, spatial reflection $x \to -x$ keeps the effective Hamiltonian Eq. (7) invariant.

This emergent Z_2 symmetry in the crossover regime has direct experimental signatures. First, as illustrated in the middle column of Fig. 2, the clouds of the minority spin component appear at both positive and negative momenta, which are of equal size. Second, one can see in Fig. 3 that for bosons, the condensation momentum $k_{\rm min} = 0$ at $\lambda = 3.04$. Third, one can see in Fig. 4 that for fermions, $\Delta k_{\rm F} = 0$ and the Fermi surface is not distorted at $\lambda = 3.06$. Both are indicated by vertical dashed lines in Figs. 3 and 4. It is remarkable to note that although Figs. 3 and 4 consider two different systems with different detuning δ, different dimensionality, and different statistics, these two values of λ agree remarkably with each other because both are determined by the underlying emergent spatial reflectional symmetry. This value is also consistent with the condition $\mathcal{J}_0(\lambda M_z/2) = \mathcal{J}_1(\lambda M_z/2)$, which gives $\lambda = 2.87$ by taking $M_z = 1$. In fact, the self-consistent M_z is close to but smaller than unity when $\Omega < 4 E_r$, with $E_{\rm r} = \hbar^2 k_{\rm r}^2/(2m)$, and the actual value of λ for the emergent Z_2 symmetry is slightly larger than 2.87.

Outlook. In the past decades, extensive studies have revealed the rich physics of ultracold atoms in the presence of a static SO coupling, whose format and strength are both fixed. This work proposes a realistic proposal to realize a density-dependent SO coupling, as given by Eq. (7). Since the density of atoms is a dynamical variable, this SO coupling has intrinsic dynamics. Here, as an important initial step to lay down the basis, we only consider the mean-field theory, but more interesting effects can certainly be found in future studies by including density fluctuations. Novel physics can be found particularly in the regime either when density fluctuations are strong, such as in interacting one-dimensional gases, or when the system is sensitive to density, such as in the crossover regime.

[1] C. Kittel, *Quantum Theory of Solids* (John Wiley and Sons, New York, 1963).

[2] R. Winkler, *Spin-Orbit Coupling Effects in Two-Dimensional Electron and Hole Systems* (Springer-Verlag, Berlin, 2003).

[3] H. Zhai, Int. J. Mod. Phys. B **26**, 1230001 (2012).

[4] N. Goldman, G. Juzeliūnas, P. Öhberg, and I. B. Spielman, Rep. Prog. Phys. **77**, 126401 (2014).

[5] H. Zhai, Rep. Prog. Phys. **78**, 026001 (2015).

[6] Y. J. Lin, K. Jiménez-García, and I. B. Spielman, Nature **471**, 83 (2011).

[7] P. Wang, Z. Q. Yu, Z. Fu, J. Miao, L. Huang, S. Chai, H. Zhai, and J. Zhang, Phys. Rev. Lett. **109**, 095301 (2012).

[8] L. W. Cheuk, A. T. Sommer, Z. Hadzibabic, T. Yefsah, W. S. Bakr, and M. W. Zwierlein, Phys. Rev. Lett. **109**, 095302 (2012).

[9] T. D. Stanescu, B. Anderson, and V. Galitski, Phys. Rev. A **78**, 023616 (2008).

[10] C. Wang, C. Gao, C. M. Jian, and H Zhai, Phys. Rev. Lett. **105**, 160403 (2010).

[11] C. M. Jian and H. Zhai, Phys. Rev. B **84**, 060508(R) (2011).

[12] T.-L. Ho and S. Zhang, Phys. Rev. Lett. **107**, 150403 (2011).

[13] C. J. Wu, I. Mondragon-Shem, and X. F. Zhou, Chin. Phys. Lett. **28**, 097102 (2011).

[14] Z. F. Xu, R. Lü, and L. You, Phys. Rev. A **83**, 053602 (2011).

[15] S. Sinha, R. Nath, and L. Santos, Phys. Rev. Lett. **107**, 270401 (2011).

[16] J.-Y. Zhang, S.-C. Ji, Z. Chen, L. Zhang, Z.-D. Du, B. Yan, G.-S. Pan, B. Zhao, Y. J. Deng, H. Zhai, S. Chen, and J.-W. Pan, Phys. Rev. Lett. **109**, 115301 (2012).

[17] T. Ozawa and G. Baym, Phys. Rev. A **85**, 013612 (2012).

[18] T. Ozawa and G. Baym, Phys. Rev. A **85**, 063623 (2012).

[19] Y. Li, L. P. Pitaevskii, and S. Stringari, Phys. Rev. Lett. **108**, 225301 (2012).

[20] G. I. Martone, Y. Li, L. P. Pitaevskii, and S. Stringari, Phys. Rev. A **86**, 063621 (2012).

[21] L. Zhang, J.-Y. Zhang, S.-C. Ji, Z. D. Du, H. Zhai, Y. Deng, S. Chen, P. Zhang, and J.-W. Pan, Phys. Rev. A **87**, 011601 (2013).

[22] R. M. Wilson, B. M. Anderson, and C. W. Clark, Phys. Rev. Lett. **111**, 185303 (2013).

[23] S. Gopalakrishnan, I. Martin, and E. A. Demler, Phys. Rev. Lett. **111**, 185304 (2013).

[24] Y. Li, G. I. Martone, L. P. Pitaevskii, and S. Stringari, Phys. Rev. Lett. **110**, 235302 (2013).

[25] Q. Zhou and X. Cui, Phys. Rev. Lett. **110**, 140407 (2013).

[26] S.-C. Ji, J.-Y. Zhang, L. Zhang, Z.-D. Du1 W. Zheng, Y.-J. Deng, H. Zhai, S. Chen, and J.-W. Pan, Nat. Phys. **10**, 1038 (2014).

[27] S.-C. Ji, L. Zhang, X.-T. Xu, Z. Wu, Y. Deng, S. Chen, and J.-W. Pan, Phys. Rev. Lett. **114**, 105301 (2015).

[28] Z. Wu, L. Zhang, W. Sun, X.-T. Xu, B.-Z. Wang, S.-C. Ji, Y. Deng, S. Chen, X.-J. Liu, and J.-W. Pan, Science **354**, 83 (2016).

[29] J. P. Vyasanakere, S. Zhang, and V. B. Shenoy, Phys. Rev. B **84**, 014512 (2011).

[30] Z. Q. Yu and H. Zhai, Phys. Rev. Lett. **107**, 195305 (2011).

[31] M. Gong, S. Tewari, and C. Zhang, Phys. Rev. Lett. **107**, 195303 (2011).

[32] H. Hu, L. Jiang, X. J. Liu, and H. Pu, Phys. Rev. Lett. **107**, 195304 (2011).

[33] P. Zhang, L. Zhang, and Y. Deng, Phys. Rev. A **86**, 053608 (2012).

[34] L. Zhang, Y. Deng, and P. Zhang, Phys. Rev. A **87**, 053626 (2013).

[35] V. B. Shenoy, Phys. Rev. A **88**, 033609 (2013).

[36] L. Han and C. A. R. Sa' de Melo, Phys. Rev. A **85**, 011606(R) (2012).

[37] K. Seo, L. Han, and C. A. R. Sa' de Melo, Phys. Rev. Lett. **109**, 105303 (2012).

[38] Z. Fu, L. Huang, Z. Meng, P. Wang, L. Zhang, S. Zhang, H. Zhai, P. Zhang, and J. Zhang, Nat. Phys. **10**, 110 (2014).

[39] L. Huang, Z. Meng, P. Wang, P. Peng, S.-L. Zhang, L. Chen, D. Li, Q. Zhou, and J. Zhang, Nat. Phys. **12**, 540 (2016).

[40] Y. Deng, J. Cheng, H. Jing, and S. Yi, Phys. Rev. Lett. **112**, 143007 (2014).

[41] J.-S. Pan, X.-J. Liu, W. Zhang, W. Yi, and G.-C. Guo, Phys. Rev. Lett. **115**, 045303 (2015).

[42] R. M. Kroeze, Y. Guo, and B. L. Lev, Phys. Rev. Lett. **123**, 160404 (2019).

[43] T. Keilmann, S. Lanzmich, I. McCulloch, and M. Roncaglia, Nat. Commun. **2**, 361 (2011).

[44] M. J. Edmonds, M. Valiente, G. Juzeliūnas, L. Santos, and P. Öhberg, Phys. Rev. Lett. **110**, 085301 (2013).

[45] S. Greschner, G. Sun, D. Poletti, and L. Santos, Phys. Rev. Lett. **113**, 215303 (2014).

[46] L. W. Clark, B. M. Anderson, L. Feng, A. Gaj, K. Levin, and C. Chin, Phys. Rev. Lett. **121**, 030402 (2018).

[47] F. Görg, K. Sandholzer, J. Minguzzi, R. Desbuquois, M. Messer, and T. Esslinger, Nat. Phys. **15**, 1161 (2019).

[48] C. Schweizer, F. Grusdt, M. Berngruber, L. Barbiero, E. Demler, N. Goldman, I. Bloch, and M. Aidelsburger, Nat. Phys. **15**, 1168 (2019).

[49] L. W. Clark, L.-C. Ha, C.-Y. Xu, and C. Chin, Phys. Rev. Lett. **115**, 155301 (2015).

[50] L. W. Clark, A. Gaj, L. Feng, and C. Chin, Nature **551**, 356 (2017).

[51] W. Zheng and H. Zhai, Phys. Rev. A **89**, 061603(R) (2014).

[52] N. Goldman, J. Dalibard, M. Aidelsburger, and N. R. Cooper, Phys. Rev. A **91**, 033632 (2015).

[53] There exists another situation that this 2ω frequency term cannot be discarded. That is, there is an interaction energy $\sim 2\omega$ resonant with the 2ω driving. This can also result in density-dependent gauge field and this situation will be reported elsewhere.